A&A 527, A95 (2011)
DOI: 10.1051/0004-6361/201015079

Astronomy & Astrophysics

Herschel observations of EXtra-Ordinary Sources (HEXOS): Methanol as a probe of physical conditions in Orion KL⋆

S. Wang[1], E. A. Bergin[1], N. R. Crockett[1], P. F. Goldsmith[2], D. C. Lis[3], J. C. Pearson[2], P. Schilke[4,5], T. A. Bell[3], C. Comito[4], G. A. Blake[6], E. Caux[7,8], C. Ceccarelli[9], J. Cernicharo[10], F. Daniel[10,11], M.-L. Dubernet[12,13], M. Emprechtinger[3], P. Encrenaz[11], M. Gerin[11], T. F. Giesen[5], J. R. Goicoechea[10], H. Gupta[2], E. Herbst[14], C. Joblin[7,8], D. Johnstone[15], W. D. Langer[2], W. B. Latter[16], S. D. Lord[16], S. Maret[9], P. G. Martin[17], G. J. Melnick[18], K. M. Menten[4], P. Morris[16], H. S. P. Müller[5], J. A. Murphy[19], D. A. Neufeld[20], V. Ossenkopf[13,21], M. Pérault[11], T. G. Phillips[3], R. Plume[22], S.-L. Qin[5], S. Schlemmer[5], J. Stutzki[5], N. Trappe[19], F. F. S. van der Tak[21], C. Vastel[7,8], H. W. Yorke[2], S. Yu[2], and J. Zmuidzinas[3]

(Affiliations can be found after the references)

Received 28 May 2010 / Accepted 21 December 2010

ABSTRACT

We have examined methanol emission from Orion KL with the *Herschel*/HIFI instrument, and detected two methanol bands centered at 524 GHz and 1061 GHz. The 524 GHz methanol band (observed in HIFI band 1a) is dominated by the isolated $\Delta J = 0$, $K = -4 \rightarrow -3$, $v_t = 0$ Q branch, and includes 25 E-type and 2 A-type transitions. The 1061 GHz methanol band (observed in HIFI band 4b) is dominated by the $\Delta J = 0$, $K = 7 \rightarrow 6$, $v_t = 0$ Q branch transitions which are mostly blended. We have used the isolated E-type $v_t = 0$ methanol transitions to explore the physical conditions in the molecular gas. With HIFI's high velocity resolution, the methanol emission contributed by different spatial components along the line of sight toward Orion KL (hot core, low velocity flow, and compact ridge) can be distinguished and studied separately. The isolated transitions detected in these bands cover a broad energy range (upper state energy ranging from 80 K to 900 K), which provides a unique probe of the thermal structure in each spatial component. The observations further show that the compact ridge is externally heated. These observations demonstrate the power of methanol lines as probes of the physical conditions in warm regions in close proximity to young stars.

Key words. ISM: abundances – ISM: molecules

1. Introduction

Methanol (CH_3OH) is an abundant molecule in a wide range of interstellar conditions (e.g., Friberg et al. 1988; Menten et al. 1988). An asymmetric-top rotor, methanol has numerous rotational transitions from far-infrared to millimeter wavelengths. This marks methanol as a common "weed" molecule, and the number and strength of its transitions means that methanol contamination has to be minimized when analyzing transitions from other molecules. However, rather than being treated solely as a contaminant, methanol is also a useful molecular tracer of dense gas (Menten et al. 1988). Leurini et al. (2004) further explore the properties of methanol emission in dense molecular clouds and illustrate how methanol transitions at sub-millimeter and millimeter wavelengths are sensitive to the density and the kinetic temperature of the gas. Therefore, with its observational advantage of a large number of lines being observable simultaneously, methanol is an excellent tool with which to probe the physical structure in dense molecular gas (also see Kama et al. 2010).

A full spectral scan toward Orion KL covering frequency ranges 479.8 to 560.0 GHz (band 1a) and 1047.0 to 1121.5 GHz (band 4b) has been carried out by the HIFI instrument (de Graauw et al. 2010) aboard on the *Herschel* Space Observatory (Pilbratt et al. 2010), as part of the guaranteed time key program *Herschel*/HIFI observations of EXtra-Ordinary Sources: the Orion and sagittarius b2 star-forming regions (HEXOS). Orion KL, located within the Orion molecular cloud at ~450 pc, is the nearest massive star-forming region (Genzel & Stutzki 1989). It contains several kinematic components (e.g., Blake et al. 1987; Persson et al. 2007), a hot core, multiple outflows, and the compact ridge, surrounding by cold quiescent gas. We have detected two methanol bands (i.e., groups of methanol lines within small frequency ranges) with transitions spanning a large range in upper state energy (80–900 K) falling within a single HIFI bandpass (4 GHz). In this paper, we show that these two bands of methanol can be used to determine the gas temperature and we explore thermal gradients in the Orion compact ridge. In Sect. 2, we discuss the HEXOS observations and the analysis tools used in this study. In Sect. 3, we present the spectra of two methanol bands and their $^{13}CH_3OH$ counterparts, and resolve the methanol emission from the compact ridge and the outflow. In Sect. 4, we show the population diagrams for the detected isolated methanol transitions for compact ridge and the outflow. And in Sect. 5, we examine how these two methanol bands can be used to provide additional information on the physical structure of the emitting regions.

2. Observations

The HIFI observations presented here, which are part of HEXOS (Bergin et al. 2010), are full spectral scans in bands 1a and 4b, covering a frequency range of 479.8 to 560.0 GHz and 1047.0 to 1121.5 GHz, respectively, pointing towards the Orion hot core

⋆ *Herschel* is an ESA space observatory with science instruments provided by European-led Principal Investigator consortia and with important participation from NASA.

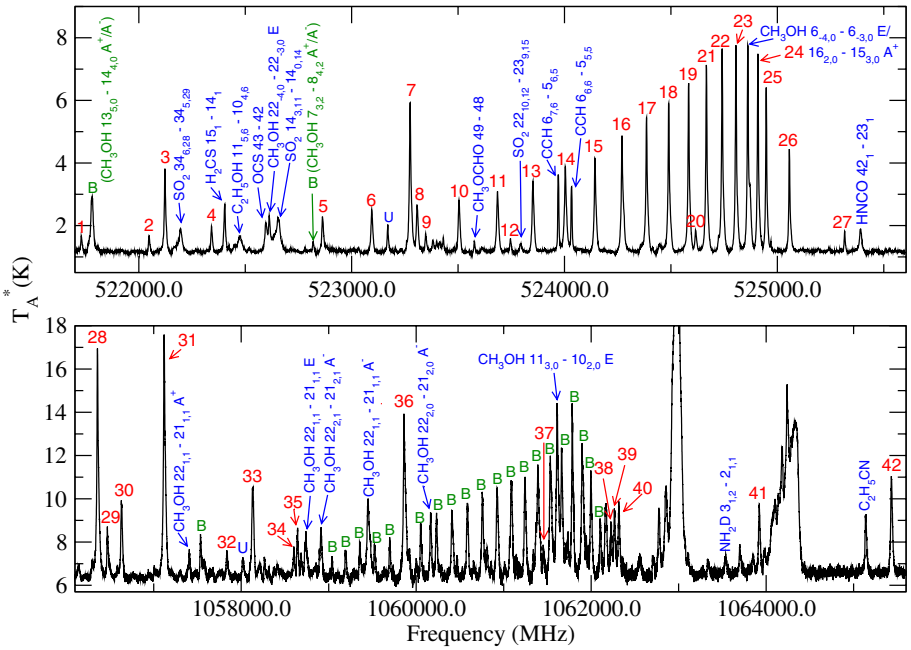

Fig. 1. HIFI spectra of two methanol bands in band 1a (521.7–525.6 GHz; *upper panel*) and 4b (1056.1–1065.6 GHz; *lower panel*). Red number 1-42 label isolated methanol transitions, which are also listed in Table 1. Blue texts label transitions from other molecules and the methanol transitions which are blended. Green texts and "B" label the methanol lines which are blended with different parity states. "U" labels two unidentified lines.

at $\alpha_{J2000} = 5^h35^m14.3^s$ and $\delta_{J2000} = -5°22'36.7''$. These observations were carried out on March 1 and 3, 2010 using the dual beam switch (DBS) mode with redundancy 6, with the wide band spectrometer (WBS) providing a spectral resolution of 1.1 MHz over a 4 GHz IF bandwidth. The HIFI beam sizes are ~43″ in band 1a and 20″ in band 4b, and the beam efficiency in both bands is 0.71. All data presented here were processed with HIPE (Ott et al. 2010) version 2.4, using the standard HIFI deconvolution (*doDeconvolution* task in HIPE). From line-free regions in the spectrum, we obtain a rms of $T_A^* = 0.065$ K for band 1a and $T_A^* = 0.116$ K for band 4b. All spectra here were analyzed using the XCLASS program (https://www.astro.uni-koeln.de/projects/schilke/XCLASS), which provides access to the CDMS and JPL molecular catalogs (Müller et al. 2001, 2005; Pickett et al. 1998) for identifying lines and obtaining the molecular parameters of methanol (Xu & Lovas 1997; Xu et al. 2008).

3. Results

3.1. Detection of distinctive methanol bands

There are 223 and 141 methanol lines with $v_t = 0$ and 1 detected in HIFI bands 1a and 4b, respectively. No molecular and frequency information for transitions with $v_t > 1$ is available at present from the CDMS and JPL catalogs. Among these detected methanol lines, 112 in band 1a and 73 in band 4b are isolated transitions. The rest are transitions which are blended with either other methanol transitions or lines of other molecules. These detected isolated methanol transitions span a wide range in upper state energy (0–1000 K). The focus of this paper is to investigate how we can utilize the advantage offered by methanol – having many transitions within small frequency ranges – to probe the physical conditions in the emitting region. For this purpose, we look for groups of isolated methanol transitions which are confined within small frequency range in the spectrum but which also cover a wide range in upper state energy with minimal line blending. This approach is useful as it shows an example of how physical conditions can be probed by observing only a limited spectral range.

Among all the detected methanol lines, there are two very distinctive methanol bands in HIFI bands 1a and 4b – both are constructed with a series of methanol lines confined within a few GHz range and have a similar characteristic spectral shape. Figure 1 shows the spectra of these two methanol bands. The first covers 521.7 to 525.6 GHz in HIFI band 1a (upper panel). The 4 GHz spectrum includes the methanol band peaked at 524.8 GHz, which is defined as the "524 GHz methanol band" in this paper. The second covers from 1056.1 to 1065.6 GHz in HIFI band 4b (lower panel). The 10 GHz spectrum includes the methanol band peaked at 1061.6 GHz, which is defined as the "1061 GHz methanol band" in this paper.

In the 524 GHz methanol band, 31 methanol lines are detected: 27 isolated methanol transitions (labeled in red numbers 1–27), 2 lines either blended with other methanol transitions or transitions from other molecules (labeled in blue), and 2 lines which are blended with methanol transitions having the same quantum numbers (J, K, v_t) but different parity with either E, A+, or A− state (defined as the blended "B" lines and labeled as "B" in green). Methanol has E and A symmetric states, which are considered as different species as no radiative transitions are allowed between them. A-type methanol can be further separated as + and − parity. Figure 1 shows that the 524 GHz methanol band is dominated by isolated transitions, which are mostly $\Delta J = 0$, $K = -4 \rightarrow -3$ Q branch with $v_t = 0$ representing the torsional ground state. On the other hand, in the 1061 GHz methanol band, 42 methanol lines are detected: 15 isolated transitions (labeled in red numbers 28–42), 6 lines blended with others, and 21 blended "B" lines. Figure 1 shows that, unlike the 524 GHz methanol band, the 1061 GHz methanol band is dominated by the blended "B" lines mostly with $\Delta J = 0$, $K = 7 \rightarrow 6$, $v_t = 0$ transitions.

Table 1 lists the molecular parameters of the 42 isolated transitions, including 37 E-type (33 $v_t = 0$ and 4 $v_t = 1$) and 5 A-type (4 $v_t = 0$ and 1 $v_t = 1$) methanol transitions, their peak intensities in units of antenna temperature (T_A^*), line frequency ν, upper state energy E_u, and $S\mu^2$ where S and μ are the line strength and dipole moment, respectively. The peak intensities are estimated with baseline continuum subtracted; the continuum level ~1.23 K for band 1a and ~6.45 K for band. These methanol lines

Table 1. Detected isolated CH_3OH Lines.

Label	CH_3OH (J_{K,v_t})	ν (MHz)	E_u (K)	$S\mu^2$ (D^2)	T_A^* (K)
1	$25_{-4,0} \rightarrow 25_{-3,0}$ E	521 728.127	841.28	22.047	0.44
2	$24_{-4,0} \rightarrow 24_{-3,0}$ E	522 046.360	783.41	21.209	0.45
3	$9_{4,0} \rightarrow 10_{3,0}$ E	522 121.802	200.44	1.997	2.58
4	$23_{-4,0} \rightarrow 23_{-3,0}$ E	522 340.009	727.83	20.360	0.74
5	$21_{-4,0} \rightarrow 21_{-3,0}$ E	522 861.608	623.60	18.646	1.05
6	$20_{-4,0} \rightarrow 20_{-3,0}$ E	523 092.856	574.94	17.773	1.28
7	$14_{-1,0} \rightarrow 0,0$ E	523 274.293	248.94	10.900	4.70
8	$19_{-4,0} \rightarrow 19_{-3,0}$ E	523 306.240	528.60	16.897	1.44
9	$24_{1,0} \rightarrow 23_{2,0}$ A^+	523 346.243	703.52	10.320	0.51
10	$18_{-4,0} \rightarrow 18_{-3,0}$ E	523 502.932	484.56	16.008	1.59
11	$17_{-4,0} \rightarrow 17_{-3,0}$ E	523 683.978	442.84	15.112	1.86
12	$24_{3,0} \rightarrow 23_{4,0}$ A^-	523 744.752	745.74	7.788	0.35
13	$16_{-4,0} \rightarrow 16_{-3,0}$ E	523 850.320	403.43	14.206	2.18
14	$15_{-4,0} \rightarrow 15_{-3,0}$ E	524 002.815	366.32	13.290	2.64
15	$14_{-4,0} \rightarrow 14_{-3,0}$ E	524 142.239	331.53	12.360	2.92
16	$13_{-4,0} \rightarrow -3,0$ E	524 269.306	299.07	11.423	3.64
17	$12_{-4,0} \rightarrow 12_{-3,0}$ E	524 384.667	268.91	10.468	4.20
18	$11_{-4,0} \rightarrow 11_{-3,0}$ E	524 488.918	241.07	9.499	4.67
19	$10_{-4,0} \rightarrow 10_{-3,0}$ E	524 582.604	215.55	8.511	5.32
20	$24_{-2,0} \rightarrow 24_{-1,0}$ E	524 614.631	724.08	20.883	0.62
21	$9_{-4,0} \rightarrow 9_{-3,0}$ E	524 666.219	192.34	7.501	5.90
22	$8_{-4,0} \rightarrow 8_{-3,0}$ E	524 740.210	171.46	6.461	6.44
23	$7_{-4,0} \rightarrow 7_{-3,0}$ E	524 804.977	152.90	5.380	6.51
24	$5_{-4,0} \rightarrow 5_{-3,0}$ E	524 908.214	122.73	3.018	6.26
25	$4_{-4,0} \rightarrow 4_{-3,0}$ E	524 947.258	111.12	1.647	5.18
26	$4_{-3,0} \rightarrow 5_{-2,0}$ E	525 055.729	85.92	0.560	3.21
27	$13_{1,0} \rightarrow 12_{-2,0}$ E	525 315.119	232.30	0.169	0.57
28	$11_{-4,0} \rightarrow 10_{-3,0}$ E	1056 354.886	241.08	8.659	10.58
29	$18_{0,1} \rightarrow 17_{1,1}$ E	1056 466.663	696.17	8.313	2.32
30	$22_{-1,0} \rightarrow 21_{-1,0}$ E	1056 627.148	590.67	17.746	3.53
31	$6_{-3,0} \rightarrow 5_{-2,0}$ E	1057 117.722	111.46	5.541	11.21
32	$22_{-2,1} \rightarrow 21_{-2,1}$ E	1057 831.005	949.39	17.720	1.19
33	$9_{-7,1} \rightarrow 8_{-6,1}$ E	1058 132.994	627.54	12.064	4.12
34	$22_{2,1} \rightarrow 21_{2,1}$ A^+	1058 598.551	883.67	17.603	1.37
35	$22_{0,1} \rightarrow 21_{0,1}$ E	1058 639.968	885.60	17.797	2.23
36	$13_{-2,0} \rightarrow 12_{-1,0}$ E	1059 858.944	237.30	6.157	7.47
37	$22_{-7,0} \rightarrow 21_{-7,0}$ E	1061 448.476	846.67	16.095	1.37
38	$22_{-5,0} \rightarrow 21_{-5,0}$ E	1062 221.782	710.72	16.893	2.44
39	$22_{3,0} \rightarrow 21_{3,0}$ A^+	1062 261.800	636.61	17.458	3.06
40	$22_{2,0} \rightarrow 21_{2,0}$ E	1062 312.231	609.56	17.571	3.41
41	$22_{2,0} \rightarrow 21_{2,0}$ A^+	1063 916.882	625.04	17.739	3.27
42	$18_{1,0} \rightarrow 17_{0,0}$ E	1065 427.650	417.93	7.792	4.51

have peak intensities between 0.4 and 12 K. They are widely spread in upper state energy, which ranges from 80 to 900 K, covering almost the same energy range as those detected from the entirety of methanol lines detected in bands 1a and 4b. This energy range is sensitive to kinetic temperatures anticipated in molecular clouds, and these lines are thus a good set of transitions to probe the cloud conditions. We only focus on those 33 isolated E-type $v_t = 0$ (25 in band 1a and 8 in band 4b), in order not to get too involved in complicated excitation issues, any potential A/E abundance variations, and any $v_t > 0$ transitions that can be excited through radiative pumping of the strong Nv_{12} torsional bands.

Furthermore, among all 112 isolated methanol lines detected in the whole of band 1a, there are in total 55 isolated E-type $v_t = 0$ transitions. This means that 25 (almost 50%) out of the total 55 lines in band 1a (covering 80 GHz) are located within the 4 GHz bandwidth of this 524 methanol band. On the other hand, among the 73 isolated methanol lines detected in whole band 4b, there are in total 36 isolated E-type $v_t = 0$ transitions – only ~20% of them are located in the 1061 GHz methanol band. The fact that the 524 GHz methanol band is dominated by isolated transitions while the 1061 GHz methanol band is mostly constructed with blended "B" lines, suggests that the 524 GHz methanol band is more suitable for exploration of the physical conditions. Hereafter, when we use the terms "524 GHz methanol band" and "1061 GHz methanol band" we are referring only to those isolated E-type $v_t = 0$ transitions.

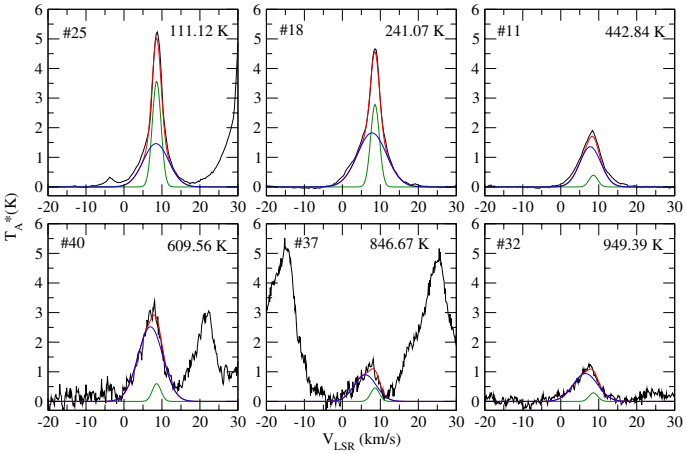

Fig. 2. Spectra of six isolated methanol lines. Each spectrum is plotted with the data (black) and the two-component Gaussian fit (red) to the data, which includes a narrower component (green) and wider component (blue). The number in the upper left corner and the energy (in K) in the upper right corner of each panel indicate the associated methanol transition and its upper state energy given in Table1.

3.2. Resolving different kinematic components in Orion KL

Figure 2 plots the spectra of six isolated methanol lines with different upper state energies. All methanol lines show asymmetry in the line profiles, indicating the existence of multiple contributions from different kinematic components in Orion KL, as suggested previously. For example, a high resolution VLA spectrum of one methanol line toward Orion KL (Wilson et al. 1989) shows one narrower (linewidth $\Delta V \sim 2$ km s^{-1}, and V_{LSR} =7.6 km s^{-1}) and one wider ($\Delta V \sim 7$ km s^{-1}, and $V_{LSR} \sim$ 6.2–9.2 km s^{-1}) component. Consistent with previous results, the detected isolated methanol lines in Table 1 can all be fit with two Gaussians (see Fig. 2): (1) a narrow component at V_{LSR} =8.6 km s^{-1} with ΔV = 2.7 km s^{-1}, and (2) one wide component at V_{LSR} = 6–9 km s^{-1} with ΔV = 4–11 km s^{-1}. Therefore, we fitted all methanol lines with fixed V_{LSR} at 8.6 km s^{-1} and ΔV at 2.7 km s^{-1} for the narrow component, and freely fitting the V_{LSR} and ΔV for the wide component. It is well known that there are distinct spatial components (hot core, outflow, and compact ridge) along the line of sight that can be distinguished by their kinematic signature in the molecular emission profile (e.g., Blake et al. 1987; Persson et al. 2007). Based on this information, we assign the V_{LSR} =8.6 km s^{-1} component to the compact ridge, and the V_{LSR} = 6–9 km s^{-1} component to the outflow.

3.3. $^{13}CH_3OH$ counterparts for those detected methanol transitions

In order to estimate the opacities of these $^{12}CH_3OH$ transitions, we look for their $^{13}CH_3OH$ counterparts throughout the whole band 1a. 13 of these 25 methanol transitions in HIFI band 1a

Table 2. Detected $^{13}CH_3OH$ counterparts.

$^{13}CH_3OH$ (J_{K,v_t})	ν (MHz)	E_u (K)	T_A^* (K)	τ_{12} (cr)	τ_{12} (outflow)
$14_{-1,0} \rightarrow 0,0$ E	507 380.068	243.11	0.58	1.5	12.9
$16_{-4,0} \rightarrow 16_{-3,0}$ E	528 323.505	396.25	0.28	16.9	4.4
$15_{-4,0} \rightarrow 15_{-3,0}$ E	528 471.541	360.05	0.34	7.8	4.2
$14_{-4,0} \rightarrow 14_{-3,0}$ E	528 606.922	326.10	0.30	7.2	6.3
$13_{-4,0} \rightarrow -3,0$ E	528 730.329	294.41	0.41	8.7	4.8
$12_{-4,0} \rightarrow 12_{-3,0}$ E	528 842.385	264.98	0.57	6.1	6.5
$11_{-4,0} \rightarrow 11_{-3,0}$ E	528 943.663	237.82	0.60	5.6	6.6
$9_{-4,0} \rightarrow 9_{-3,0}$ E	529 115.969	190.27	0.70	5.7	7.3
$8_{-4,0} \rightarrow 8_{-3,0}$ E	529 187.882	169.89	0.70	4.5	9.7
$5_{-4,0} \rightarrow 5_{-3,0}$ E	529 351.258	122.33	0.62	5.3	8.2
$4_{-4,0} \rightarrow 4_{-3,0}$ E	529 389.156	111.00	0.65	6.4	3.5

with $E_u < 37$ K have $^{13}CH_3OH$ counterparts detected (Table 2). We did not search $^{13}CH_3OH$ for those transitions in 4b because no molecular information of $^{13}CH_3OH$ transitions with frequency above 1 THz are available in either the CDMS and JPL catalogs. Figure 3 plots four selected methanol lines and their $^{13}CH_3OH$ counterparts. Following the same strategy to separate different kinematic components as shown in Sect. 3.2, we then obtain the spectra for the compact ridge and the outflow component of each $^{13}CH_3OH$ line. By comparing CH_3OH and $^{13}CH_3OH$ lines, optical depth (τ) for compact ridge and outflow components can be estimated using

$$\frac{T_{12}}{T_{13}} = \frac{T_{ex,12}(1 - e^{-\tau_{12}})}{T_{ex,13}(1 - e^{-\tau_{13}})}, \quad (1)$$

where we have assumed that CH_3OH and $^{13}CH_3OH$ have the same excitation temperature, CH_3OH is optically thick, and $\tau_{13} = \tau_{12}/f$, where f is the 13C to 12C abundance ratio ~60 (e.g., Sheffer et al. 2007). T_{12} and T_{13} are the observed peak intensity for CH_3OH and $^{13}CH_3OH$ lines. Table 2 gives the estimated CH_3OH τ_{12} for the compact ridge and the outflow, and we see that they are mostly <10. We also estimate an upper limit of $\tau_{12} \sim 15$ for those methanol lines with $E_u > 370$ K using the three times of the the band 1a rms (rms: $T_A^* = 0.065$ K) as the upper limit for all undetected $^{13}CH_3OH$ emissions.

4. Population diagrams of the isolated transitions

Population diagrams are one traditional, but effective, way to display the relative populations of different energy states, generally obtained from a set of observed transitions (Goldsmith & Langer 1999). This is a useful tool to study the physical conditions in the gas, as the relative populations of different states change as a function of kinetic temperature and density. A population diagram plots the upper state energy E_u as the x axis and the logarithm of N_u/g_u as the y axis, where N_u and g_u are the column density and statistical weight in the upper state, respectively. N_u can be derived from the observed integrated line intensity of the associated transition with Eq. (9) in Goldsmith & Langer (1999). Therefore, if all energy levels are thermalized with single kinetic temperature (LTE), the population diagram should be a straight line with the slope and y-intercept presenting the kinetic temperature and total column density.

Figure 4 shows the population diagrams, without correcting for possible beam dilution and opacity, for the detected isolated 33 transitions of E-type $v_t = 0$ methanol and their $^{13}CH_3OH$ counterparts for the compact ridge (upper panel) and the outflow

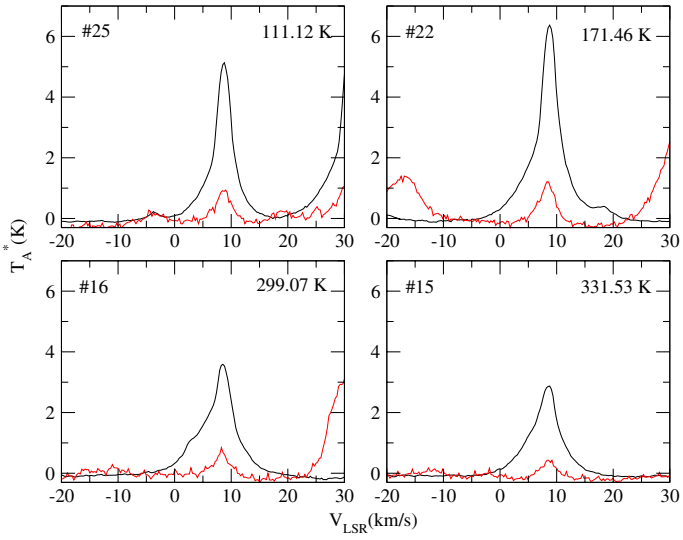

Fig. 3. Spectra of four isolated methanol lines (black) plotted with their $^{13}CH_3OH$ counterparts (red), which are scaled by a factor of two in order to be compared to methanol lines more clearly. The number in the upper left corner and the energy (in K) in the upper right corner of each panel indicate the associated methanol transition and its upper state energy given in Table 1.

(lower panel), respectively. The straight lines shown in this figure are the slopes determined from least squares fitting with a linear function. We do not include the HIFI band 4b transitions in the fitting as they are observed with different beam sizes. This figure shows that a curvature in the methanol population diagram is clearly seen for the compact ridge, which will be further examined in Sect. 5. However, there are not enough $^{13}CH_3OH$ transitions to confirm whether this curvature is also shown for $^{13}CH_3OH$ in compact ridge.

Unlike the curvature seen in the compact ridge data, the populations of the 1a transitions from the outflow can be satisfactorily represented by a single kinetic temperature in LTE of 184 K and 94 K for CH_3OH and $^{13}CH_3OH$, respectively. The $^{13}CH_3OH$ temperature might be a better approximation to the true kinetic temperature in this system because its emission is optically thin. However, the level populations derived from transitions within the 1061 GHz methanol band arising from the outflow exhibit a higher degree of scatter compared to those from compact ridge. This might suggest that the higher spatial resolution observations at 1 THz are less well coupled to the outflow and perhaps are contaminated by emission from other components such as the hot core. It is intriguing that the outflow in Orion KL is consistent with a single gas temperature, as outflow shocks are thought to be gas composed of a range of temperatures. It is likely that the derived temperature is simply showing an average gas temperature in this system.

In addition, in order to verify whether the curvature in the compact ridge and the single temperature population in the outflow are still valid for those transitions outside the selected distinctive methanol bands, we compare the population diagram of the 524 GHz methanol band with that from the 30 isolated E-type $v_t = 0$ transitions in HIFI band 1a. Figure 5 plots the population diagrams for the 524 GHz methanol band (in black) and the rest 30 lines (in red). A curvature is still present in compact ridge and all the level populations in the outflow can still be fitted with a straight line. The fitted straight lines indicating rotation temperatures of 125 and 184 K from Fig. 4 are plotted for comparison. This figure also shows that the addition of these

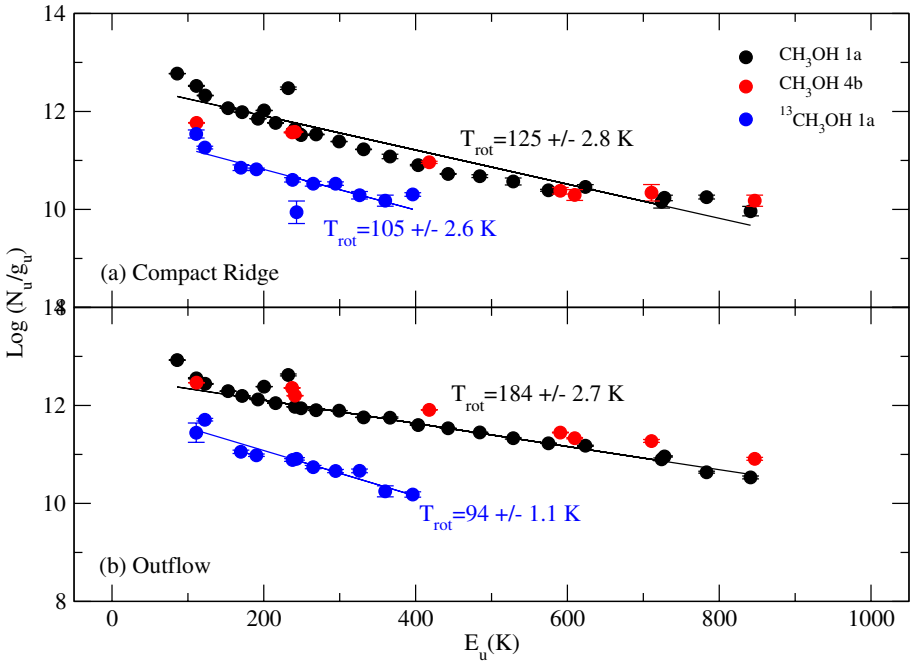

Fig. 4. Population diagrams of detected 33 E-type v_t = 0 methanol transitions for **a)** the compact ridge and **b)** the outflow. Transitions in HIFI bands 1a and 4b are plotted in black and red, respectively. Transitions of $^{13}CH_3OH$ are plotted in blue. Straight lines are fitted in order to obtain temperature estimates assuming LTE.

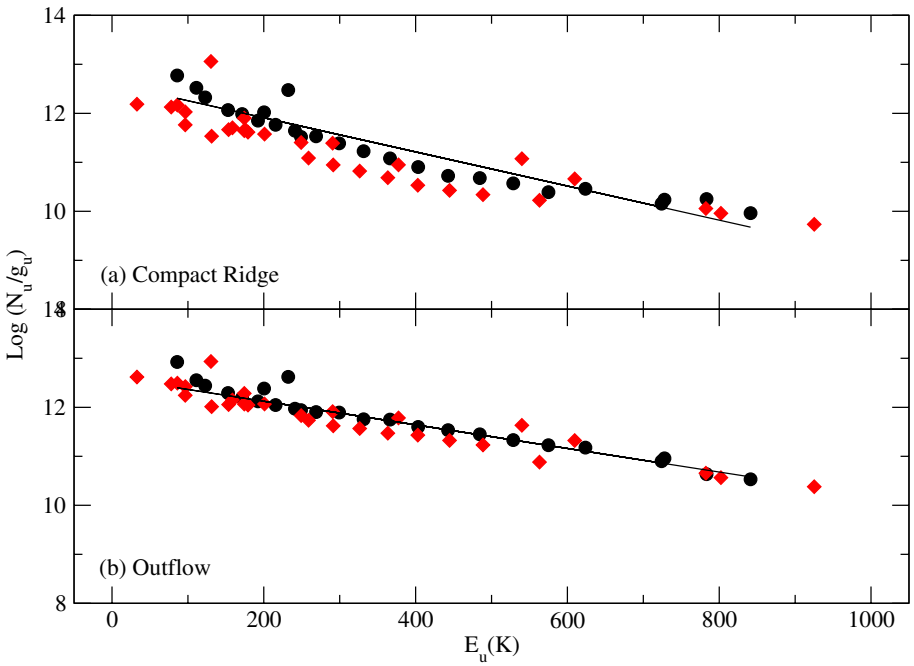

Fig. 5. Population diagrams of the 524 GHz methanol band (in black) and the other 30 isolated E-type methanol transitions detected throughout the rest of 1a (in red), for (a) the compact ridge and (b) the outflow, respectively. The fitted straight lines from Fig. 4 are also plotted for comparison.

30 transitions increases the scatter in the population diagram for both compact ridge and outflow. As these 30 transitions are actually dominated by different Q branches, compared to those in the 524 GHz methanol band, this scatter is possibly due to a deviation from LTE for populations within different K ladders.

5. Probing the thermal structure in the Orion KL compact ridge

As shown is Sect. 4, a curvature is present in the methanol population diagram of compact ridge, which cannot be fitted well with LTE excitation at a single temperature (Fig. 4). It has also been suggested in Fig. 5 that non-LTE excitation exists for methanol in the compact ridge, at least between transitions with different K ladders. Indeed, Leurini et al. (2004) has shown that LTE can be a poor assumption for methanol even in clouds with high densities. However, to date, only transitions with up to upper state energies ~350 K have available collision rates for any non-LTE modeling; while the 524 GHz methanol band includes upper state energies from 80 to 900 K. In addition, according to Fig. 4, 0−350 K is not a wide enough energy range to clearly distinguish a curve from a straight line in the population diagram.

Nevertheless, despite the currently limited capability for any non-LTE excitation modeling for all the detected transitions in the 524 GHz methanol band, it is intriguing that their population diagram shows such a cohesive curvature for compact ridge. This curvature might suggest presences of large opacity variations, thermal gradients, and/or non-LTE excitation. Indeed, the opacity estimation in Sect. 3.3 (also see Table 2) is not negligible and can indeed affect the population diagram slope. In addition, thermal gradients are another potential contributor to

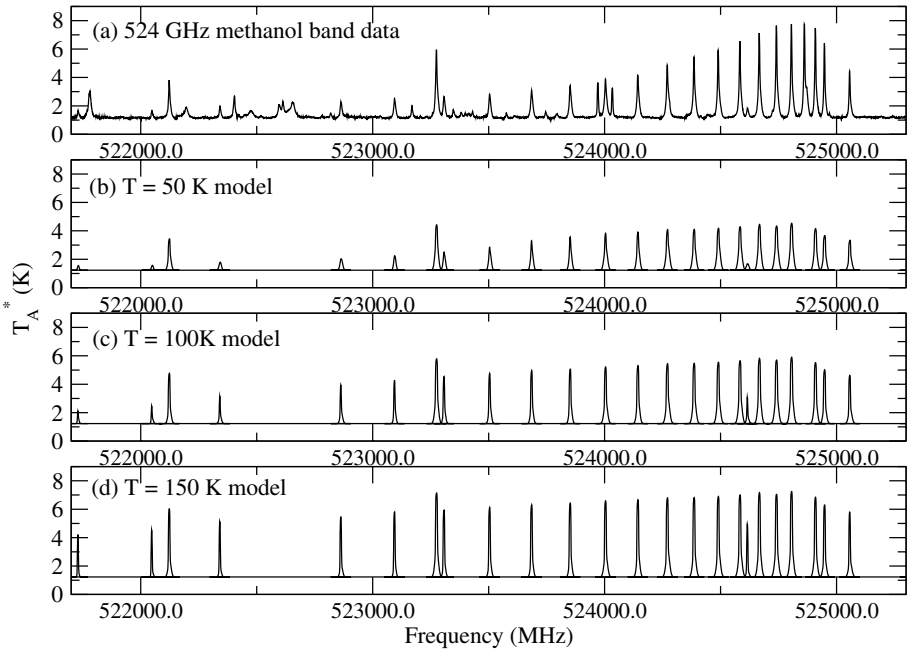

Fig. 6. Modeled spectra compared with the those observed in the 524 GHz methanol band (panel **a**), for models with constant temperature of 50 (panel **b**), 100 (panel **c**), and 150 K (panel **d**), assuming the compact ridge is a spherical clump 5″ in radius (r), constant molecular hydrogen number density 10^7 cm^{-3}, and methanol abundance 10^{-6}.

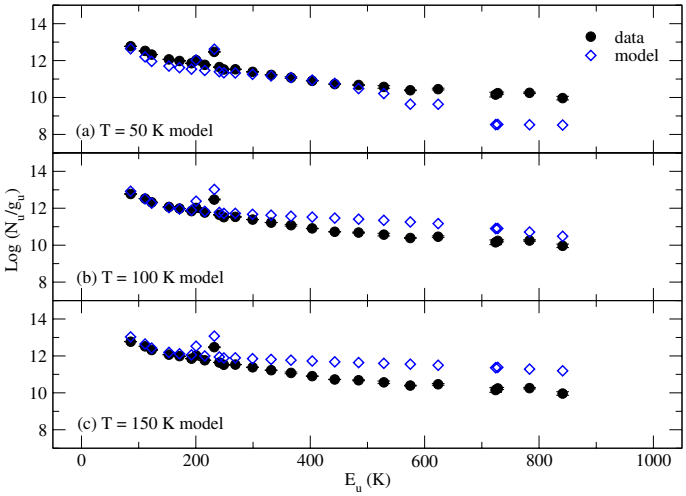

Fig. 7. Population diagrams of the observed 524 GHz methanol band (in black) and those models (in blue) shown in Fig. 6.

this observed curvature. It has been suggested that the compact ridge is externally heated due to its very narrow linewidth and high temperature, inconsistent with normal centrally heated star-forming cores (Blake et al. 1987).

In order to investigate how temperature gradients impact the curvature in a population diagram, we assume the compact ridge to be a spherical clump 5″−10″ in radius (r), having constant molecular hydrogen number density of 10^7 cm^{-3}, and a constant methanol fractional abundance of 10^{-5}−10^{-7}, as previously suggested (e.g., Beuther et al. 2006; Persson et al. 2007). We consider various radial temperature profiles, and at each given point in the modeled clump, all energy levels are assumed to be populated in LTE with the temperature appropriate for that radius. With given level populations thus determined, we then use the ray propagation part of 1D RATRAN program (Hogerheijde & van der Tak 2000) to generate a synthetic spectrum for the 524 GHz methanol band observed with a 40″ beam, consistent with the beam size in HIFI band 1a.

Figures 6 and 7 plot models with constant temperatures, to illustrate how the shape of this 524 GHz methanol band and its population diagram varies with different temperatures. Each modeled spectrum is constructed by combining the modeled compact ridge spectrum with the observed outflow spectrum. These two plots show that the observed spectrum cannot be explained by a constant temperature in LTE.

We next explore two approaches with nonuniform temperatures: central heating and external heating. First, we examine whether a centrally-heated source can result in the observed spectrum with a temperature range from a few hundred K in the center of the clump decreasing to 30−50 K in its outer layer, which is consistent with the quiescent gas temperature along the line of sight (Bergin et al. 1994). We allow any methanol abundance variation within the range 10^{-5} to 10^{-7}. We were unable to find any models within these parameter ranges that provided a satisfactory match to the observed spectrum. The cold layer in the outer part of the clump always results in large opacities which produce much optically thicker lines than are observed.

Second, we considered the possibility of externally-heated clumps and obtained a good fit that can reproduce the observed spectrum of the 524 GHz methanol band. The best fit is to a model of the compact ridge as a 7.5″ (0.016 pc) spherical clump with a constant molecular hydrogen number density of 10^7 cm^{-3}, a temperature profile with constant 30 K for $r < 5.0''$, $T \sim r^{3.8}$ outside $r > 5.0''$, and a constant methanol abundance of 3×10^{-6} and 3×10^{-7} in the inner and outer part of the clump. This corresponds to a methanol column density of 9.5×10^{18} cm^{-2} and 9.5×10^{17} cm^{-2} in the inner and outer part of the clump, respectively. This gives a temperature of 120 K on the clump surface. We stress that the assumed temperature profile in this model is not based on any self-consistent calculation, but rather is a way to explore the range of gradients needed to obtain the observed level populations. PDR models do show that gas heating can produce such sharp gradients as modelled here (Kaufman et al. 1999) and in the future we will examine more physically-motivated solutions. Figure 8 plots the 524 GHz methanol band spectrum and the modeled spectrum for this best fit externally-heated solution in panel (a) and (b), respectively,

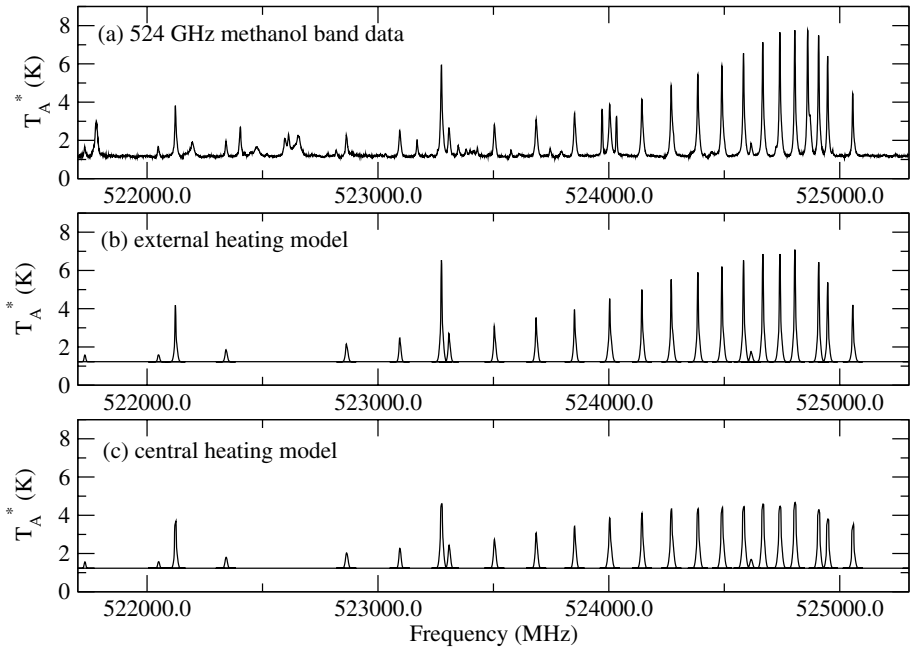

Fig. 8. **a)** The 524 GHz methanol band spectrum. **b)** The best fit externally heated modeled spectrum. **c)** Modeled spectrum of a centrally heated clump with temperature decreasing from 140 K in the center to 30 K on the clump surface.

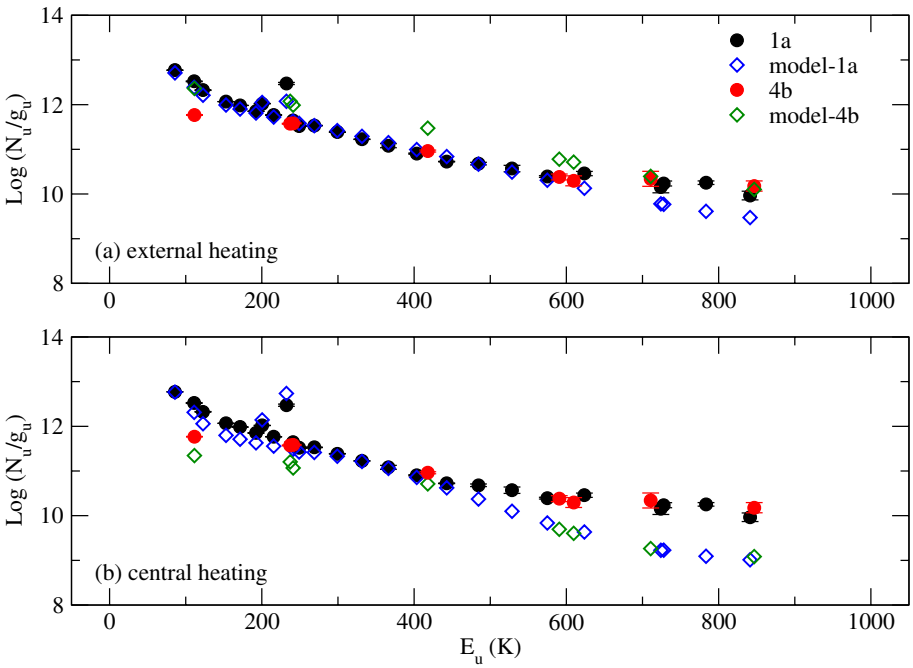

Fig. 9. **a)** Population diagrams for the HIFI band 1a (the 524 GHz methanol band, in black) and HIFI band 4b (the 1061 GHz methanol band, in red) methanol bands and the best fit externally heated model for HIFI band 1a transitions (in blue) and HIFI band 4b transitions (in green). **b)** Population diagrams for the HIFI band 1a (the 524 GHz methanol band, in black) and HIFI band 4b (the 1061 GHz methanol band, in red) methanol bands and the centrally heated model (1a in blue and 4b in green) for a clump with temperature decreasing from 140 K in the center to 30 K on the clump surface.

and their associated population diagrams in Fig. 9a. We also apply this model for transitions detected in HIFI band 4b to generate its synthetic spectrum appropriate for a 20″ beam, and further produce its population diagram shown in Fig. 9a. Figures 8c and 9b plot the modeled spectrum and its associated population diagram for one of the internally heated models we tested, for comparison, in order to show that the internally heated models can not explain the observed spectrum.

We conclude that the compact ridge is externally heated with the warm clump surface in front of the cold gas along the line of sight in LTE. Although our results show an external heated cloud can indeed result in a curvature in the observed population diagram, non-LTE excitation, such as far-infrared pumping, is also a possible contributor, which could potentially improve the fit for transitions having higher upper state energies.

6. Conclusions

We have examined the methanol emission in HIFI bands 1a and 4b from our spectral scan observations toward Orion KL. In bands 1a and 4b, 223 and 141 methanol lines are identified. In band 1a, 112 out of the total 223 lines, and in band 4b, 73 out of the 141 lines are isolated transitions. In order to minimize the confusion due to any blends, abundance variation between E- and A-type methanol, and optically pumping effects for v_t>0 transitions, we have focused on the isolated E-type v_t = 0 transitions within two methanol bands: methanol is known to have numerous transitions from far-infrared to millimeter regime, often including different symmetric states (A and E), parities, and torsional states, and blends. This makes the modeling and interpretation of underlying physical conditions difficult. But with the approach in this paper – focusing on one type of isolated

methanol transitions – methanol can be a very useful tool to probe the physical conditions in molecular clouds. In particular, the 524 GHz methanol band, including 25 isolated E-type $v_t = 0$ transitions with upper state energy ranging from 80 to 900 K, provides a valuable set of lines that can be easily observed simultaneously and used to examine the temperature and other physical conditions. Furthermore, by resolving emission from different kinematic components (compact ridge and outflow) for each transition, we find a curved slope in the population diagram for the methanol emission from the compact ridge. We suggest that this can be explained by externally heating. Unlike the compact ridge, the population diagram of the outflow component shows a highly linear relation, suggesting a single temperature, but which might be the average temperature of the outflowing gas. Our study has shown that, with HIFI's broad instantaneous frequency coverage, these methanol bands can be very useful for probing the structure of molecular clouds having various physical conditions.

Acknowledgements. HIFI has been designed and built by a consortium of institutes and university departments from across Europe, Canada and the United States under the leadership of SRON Netherlands Institute for Space Research, Groningen, The Netherlands and with major contributions from Germany, France and the US. Consortium members are: Canada: CSA, U. Waterloo; France: CESR, LAB, LERMA, IRAM; Germany: KOSMA, MPIfR, MPS; Ireland, NUI Maynooth; Italy: ASI, IFSI-INAF, Osservatorio Astrofisico di Arcetri– INAF; The Netherlands: SRON, TUD; Poland: CAMK, CBK; Spain: Observatorio Astronmico Nacional (IGN), Centro de Astrobiologa (CSIC-INTA). Sweden: Chalmers University of Technology – MC2, RSS & GARD; Onsala Space Observatory; Swedish National Space Board, Stockholm University – Stockholm Observatory; Switzerland: ETH Zurich, FHNW; USA: Caltech, JPL, NHSC. The HEXOS team also is grateful to the HIFI instrument team for building a fantastic instrument. Support for this work was provided by NASA through an award issued by JPL/Caltech.

References

Bergin, E. A., Goldsmith, P. F., Snell, R. L., & Ungerechts, H. 1994, ApJ, 431, 674
Bergin, E. A., Phillips, T. G., Comito, C., et al. 2010, A&A, 521, L20
Beuther, H., Zhang, Q., Reid, M. J., et al. 2006, ApJ, 636, 323
Blake, G. A., Sutton, E. C., Masson, C. R., & Phillips, T. G. 1987, ApJ, 315, 621
de Graauw, T., Helmich, F. P., Phillips, T. G., et al. 2010, A&A, 518, L6
Friberg, P., Hjalmarson, A., Madden, S. C., & Irvine, W. M. 1988, A&A, 195, 281
Genzel, R., & Stutzki, J. 1989, ARA&A, 27, 41
Goldsmith, P. F., & Langer, W. D. 1999, ApJ, 517, 209
Hogerheijde, M. R., & van der Tak, F. F. S. 2000, A&A, 362, 697
Kama, M., Dominik, C., Maret, S., et al. 2010, A&A, 521, L39
Kaufman, M. J., Wolfire, M. G., Hollenbach, D. J., & Luhman, M. L. 1999, ApJ, 527, 795
Leurini, S., Schilke, P., Menten, K. M., et al. 2004, A&A, 422, 573
Menten, K. M., Walmsley, C. M., Henkel, C., & Wilson, T. L. 1988, A&A, 198, 253
Müller, H. S. P., Thorwirth, S., Roth, D. A., & Winnewisser, G. 2001, A&A, 370, L49
Müller, H. S. P., Schlöder, F., Stutzki, J., & Winnewisser, G. 2005, J. Mol. Struct., 742, 215
Ott, S., Science Centre, H., & Space Agency, E. 2010, in ASP Conf. Ser., Astronomical Data Analysis Software and Systems XIX, Y. Mizumoto, K.-I. Morita, and M. Ohishi, eds., in press
Persson, C. M., Olofsson, A. O. H., Koning, N., et al. 2007, A&A, 476, 807
Pickett, H. M., Poynter, I. R. L., Cohen, E. A., et al. 1998, J. Quant. Spectros. Rad. Trans., 60, 883
Pilbratt, G. L., Riedinger, J. R., Passvogel, T., et al. 2010, A&A, 518, L1
Sheffer, Y., Rogers, M., Federman, S. R., Lambert, D. L., & Gredel, R. 2007, ApJ, 667, 1002
Wilson, T. L., Johnston, K. J., Henkel, C., & Menten, K. M. 1989, A&A, 214, 321
Xu, L., & Lovas, F. J. 1997, J. Phys. Chem. Ref. Data, 26, 17
Xu, L., Fisher, J., Lees, R. M., et al. 2008, J. Mol. Spectr., 251, 305

[1] Department of Astronomy, University of Michigan, 500 Church Street, Ann Arbor, MI 48109, USA
e-mail: shiya@umich.edu
[2] Jet Propulsion Laboratory, Caltech, Pasadena, CA 91109, USA
[3] California Institute of Technology, Cahill Center for Astronomy and Astrophysics 301-17, Pasadena, CA 91125, USA
[4] Max-Planck-Institut für Radioastronomie, Auf dem Hügel 69, 53121 Bonn, Germany
[5] I. Physikalisches Institut, Universität zu Köln, Zülpicher Str. 77, 50937 Köln, Germany
[6] California Institute of Technology, Division of Geological and Planetary Sciences, MS 150-21, Pasadena, CA 91125, USA
[7] Centre d'étude Spatiale des Rayonnements, Université de Toulouse [UPS], 31062 Toulouse Cedex 9, France
[8] CNRS/INSU, UMR 5187, 9 avenue du Colonel Roche, 31028 Toulouse Cedex 4, France
[9] Laboratoire d'Astrophysique de l'Observatoire de Grenoble, BP 53, 38041 Grenoble, Cedex 9, France
[10] Centro de Astrobiología (CSIC/INTA), Laboratiorio de Astrofísica Molecular, Ctra. de Torrejón a Ajalvir, km 4 28850, Torrejón de Ardoz, Madrid, Spain
[11] LERMA, CNRS UMR8112, Observatoire de Paris and École Normale Supérieure, 24 Rue Lhomond, 75231 Paris Cedex 05, France
[12] LPMAA, UMR7092, Université Pierre et Marie Curie, Paris, France
[13] LUTH, UMR8102, Observatoire de Paris, Meudon, France
[14] Departments of Physics, Astronomy and Chemistry, Ohio State University, Columbus, OH 43210, USA
[15] National Research Council Canada, Herzberg Institute of Astrophysics, 5071 West Saanich Road, Victoria, BC V9E 2E7, Canada
[16] Infrared Processing and Analysis Center, California Institute of Technology, MS 100-22, Pasadena, CA 91125, USA
[17] Canadian Institute for Theoretical Astrophysics, University of Toronto, 60 St George St, Toronto, ON M5S 3H8, Canada
[18] Harvard-Smithsonian Center for Astrophysics, 60 Garden Street, Cambridge MA 02138, USA
[19] National University of Ireland Maynooth. Ireland
[20] Department of Physics and Astronomy, Johns Hopkins University, 3400 North Charles Street, Baltimore, MD 21218, USA
[21] SRON Netherlands Institute for Space Research, PO Box 800, 9700 AV, Groningen, The Netherlands
[22] Department of Physics and Astronomy, University of Calgary, 2500 University Drive NW, Calgary, AB T2N 1N4, Canada